Available online at www.sciencedirect.com
ScienceDirect
Journal of Sound and Vibration 301 (2007) 718–738
JOURNAL OF SOUND AND VIBRATION
www.elsevier.com/locate/jsvi

Numerical modelling of ground-borne noise and vibration in buildings due to surface rail traffic

P. Fiala[a,b,*], G. Degrande[b], F. Augusztinovicz[a]

[a] *Vibroacoustics and Audio Laboratory, Budapest University of Technology and Economics, Magyar tudósok körútja 2, H-1117 Budapest, Hungary*

[b] *Department of Civil Engineering, K.U.Leuven, Kasteelpark Arenberg 40, B-3001 Leuven, Belgium*

Received 30 June 2006; received in revised form 18 October 2006; accepted 25 October 2006
Available online 18 December 2006

Abstract

This paper deals with the numerical computation of the structural and acoustic response of a building to an incoming wave field generated by high-speed surface railway traffic. The source model consists of a moving vehicle on a longitudinally invariant track, coupled to a layered ground modelled with a boundary element formulation. The receiver model is based on a substructuring formulation and consists of a boundary element model of the soil and a finite element model of the structure. The acoustic response of the building's rooms is computed by means of a spectral finite element formulation. The paper investigates the structural and acoustic response of a multi-story portal frame office building up to a frequency of 150 Hz to the passage of a Thalys high-speed train at constant velocity. The isolation performance of three different vibration countermeasures: a floating-floor, a room-in-room, and base-isolation, are examined.

1. Introduction

Traffic induced vibrations in dense urban environments can cause annoyance to the inhabitants of surrounding buildings in the form of vibrations or re-radiated noise. Therefore, the prediction of ground-borne noise and vibration in buildings is of high importance.

The present paper discusses numerical methods used to model ground-borne structural vibrations and noise induced by surface railway traffic. A three-dimensional (3D) deterministic approach is used and the whole vibration path is discussed, starting from vibration generation by a moving high-speed train and ending with the ground-borne noise in enclosures of a building. As not only structural vibrations but also noise radiation is investigated, the upper frequency limit of computations is 150 Hz.

The problem can be divided into three weakly coupled subproblems. The first subproblem is the computation of free field ground displacements induced by the passage of a high-speed train on a longitudinally invariant track. At this step, it is assumed that the distance between the railway track and the building is large enough, so the presence of the building does not have any effect on the vibration generation

*Corresponding author.
E-mail address: fiala@hit.bme.hu (P. Fiala).

0022-460X/$ - see front matter © 2006 Elsevier Ltd. All rights reserved.
doi:10.1016/j.jsv.2006.10.019

mechanism. Several authors recently published about coupled train–track–soil models able to predict the incident wave field generated by moving sources. The track is often represented by an infinite beam supported by distributed springs [1], a layered infinite beam model [2], or a finite element model [3]. For the modelling of the underlying ground, homogeneous half-space models [1] or layered half-space models [2,4,5] are frequently used. In the present paper, the model of Lombaert et al. is used for the computation of the incident wave field. This model has been originally developed for the prediction of road traffic induced vibrations [6–8], and has been extended to handle the case of (high-speed) train excitation [9]. The model consists of a lumped parameter vehicle model, infinite beams modelling the track, and a boundary element method based on the Green's functions of a layered half-space to model the ground. The model accounts for the dynamic interaction between the train, the track and the soil.

In the second subproblem, the incident wave field is applied as an excitation to a coupled soil–structure model in order to compute structural vibrations in the nearby building. At this step, it is assumed that the presence of the acoustic field inside the building's rooms does not influence the walls' vibrations. This assumption is valid, because the impedance of the air inside the room is usually much smaller than the impedance of the vibrating walls. The applied soil–structure interaction model is based on the substructuring formulation proposed by Aubry et al. [10] and Clouteau [11], and consists of a boundary element model for the ground with the Green's functions of a layered half-space and a finite element model of the structure. This dynamic soil–structure interaction model has been successfully validated recently for the case of road traffic induced structural vibrations [12–14].

In the third subproblem, the computed structural displacements are finally used as vibration input for the computation of ground-borne noise in the building's enclosures. For typical room dimensions in office buildings or family dwellings, the targeted frequency range is relatively low, as the upper frequency limit is not much higher than the eigenfrequency of the first few acoustic room modes. Therefore, deterministic methods can be used to solve the boundary value problem of sound radiation into a closed space. Acoustic finite elements provide a straightforward method to solve the boundary value problem. As an alternative, the acoustic boundary element method can be used to compute the internal sound field [15]. This results in a smaller mesh, as the problem dimension is reduced by one. However, the conventional BE formulation based on the Green's function of an acoustic full space, results in a fully populated, frequency dependent system of equation, making the solution procedure computationally expensive. These difficulties can be avoided by using the Green's functions of the room and by formulating a direct integral representation of the internal sound pressure in terms of the walls' velocities. In this form, the boundary element method can provide a more efficient solution than finite elements. Recently, in the framework of the CONVURT (control of noise and vibrations from underground railway traffic) project [16], a Rayleigh integral based method has been developed and validated for the case of underground railway induced noise in rooms [17]. This method can be efficiently used in rectangular rooms with high wall absorption, where the sound pressure is significantly attenuated after a few reflections on the rooms walls. In the present paper, a spectral finite element method is applied to the acoustic problem. This method can also lead to a direct boundary integral representation of the internal pressure, and it is a good alternative of the Rayleigh method for rectangular rooms and for the case of low wall absorption.

As a numerical example, ground-borne noise and vibrations in a portal frame office building due to the passage of a Thalys high-speed train are considered. The necessity of the weak coupling between the incident wave field and the structure (dynamic soil–structure interaction) on the structural vibrations and ground-borne sound is investigated. The model is further used to investigate the effectiveness of vibration and noise isolation methods.

The structure of the text is as follows: Section 2 describes the methodology used to compute the incident wave field due to the passage of a high-speed train. This section presents numerical results corresponding to the passage of a Thalys high-speed train on an invariant track lying on a homogeneous half-space. Section 3 describes the soil–structure interaction model and considers the methodology used for computing the structural response. In this section, the three-story portal frame office building is introduced, and the vibration levels in different stories of the building due to the passage of the Thalys train are discussed. Section 4 describes the numerical model for the computation of the ground-borne noise. In this section, the effect of three different vibration counter measures, a floating floor, a box-within-box arrangement and base isolation is investigated.

2. The incident wave field

The model of a moving vehicle on a longitudinally invariant track is used to compute the incident wave field. The invariance of the track in the longitudinal y-direction enables to transform the spatial variable y into the longitudinal wavenumber k_y by means of a Fourier transform and compute the response to moving loads in the frequency-wavenumber domain [18].

The vehicle is modelled by a set of concentrated masses, representing the train's axles, connected to the track by Hertzian springs. The invariant track is modelled by a pair of Euler beams representing the rails, distributed spring–dampers representing the railpads, distributed mass for the sleepers and a spring–damper system for the ballast layer, as shown in Fig. 1. The track is laying on a horizontally layered soil, characterized by its shear wave velocity C_S, dilatational wave velocity C_P, material density ρ, and hysteretic material damping ratio β for each homogeneous layer.

First, the vehicle–track interaction problem is solved in a frame of reference that is moving with the train velocity v along the invariant direction y. The compliance matrices of the vehicle $\hat{\mathbf{C}}^v(\omega)$ and the track–soil system $\hat{\mathbf{C}}^t(\omega)$ are written in the moving frame of reference. These matrices are used to compute the dynamic axle loads $\hat{\mathbf{g}}(\omega)$ arising due to the rail unevenness $\hat{\mathbf{u}}_{w/r}(\omega)$ as

$$[\hat{\mathbf{C}}^v(\omega) + \hat{\mathbf{C}}^t(\omega)]\hat{\mathbf{g}}(\omega) = -\hat{\mathbf{u}}_{w/r}(\omega). \tag{1}$$

The elements of the vector $\hat{\mathbf{u}}_{w/r}(\omega)$ give the frequency content of the unloaded rail's roughness at the location of the train's axles in the moving coordinate system, while the elements of the vector $\hat{\mathbf{g}}(\omega)$ are the forces acting on the coupled track–soil model, as shown in Fig. 1.

The soil's impedance, which is incorporated in the track–soil compliance matrix, is computed in the frequency-wavenumber domain by means of a boundary element method [6] using the Green's functions of a layered half-space [19].

In a second phase, the free field soil vibrations due to a set of moving axle loads $\hat{g}_k(\omega)$ are computed in the frequency-wavenumber domain [6]:

$$\tilde{u}_{si}(x, k_y, z, \omega) = \sum_{k=1}^{n} \hat{g}_k(\omega - k_y v)\tilde{h}_{zi}(x, k_y, z, \omega)\mathrm{e}^{\mathrm{i}k_y y_k}, \tag{2}$$

where $\tilde{h}_{zi}(x, k_y, z, \omega)$ is the transfer function in the frequency-wavenumber domain between a load on the track at position $y = 0$ and a point in the far field at coordinates $\{x, z\}$, and n denotes the number of axles. The response in the spatial-time domain is then obtained by applying a double inverse Fourier transform.

A Thalys high-speed train [9,20] traveling with a velocity $v = 80\,\mathrm{m/s}$ on an uneven rail is modelled. The 200 m long train consists of two locomotives and eight carriages, having a total number of 26 axles distributed over 13 bogies. Each axle is modelled by a concentrated mass of 2027 kg.

The track is modelled as a single ballasted track. The rail has a bending stiffness of $6.489 \times 10^6\,\mathrm{Nm}^2$ and a mass of 60.8375 kg/m.

The sleepers, the resilient railpads and the ballast are modelled by smeared mass, springs and dashpots. The sleepers' dimensions are $2.5 \times 0.24 \times 0.21\,\mathrm{m}$, the sleeper distance is 0.6 m, and the smeared sleeper mass is 525 kg/m. The railpad stiffness is $235.6 \times 10^6\,\mathrm{N/m}^2$ and the railpad damping is $25.1 \times 10^3\,\mathrm{Ns/m}^2$. The ballast mass is 1750 kg/m, the ballast stiffness is $125.8 \times 10^6\,\mathrm{N/m}^2$, while the ballast damping is $41.3 \times 10^3\,\mathrm{Ns/m}^2$. The

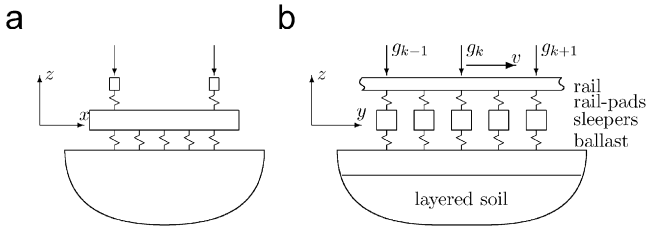

Fig. 1. (a) Cross section of the track, in the x–z plane and (b) longitudinal section in the y–z plane.

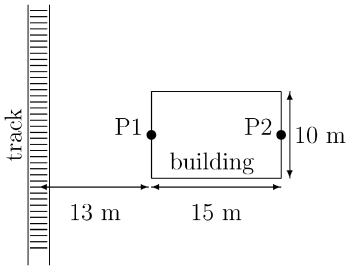

Fig. 2. Ground plan of the site.

underlying soil is modelled as a homogeneous half-space with a shear wave velocity $C_S = 250\,\mathrm{m/s}$, a compressional wave velocity $C_P = 500\,\mathrm{m/s}$, a mass density $\rho = 1750\,\mathrm{kg/m^3}$ and a material damping coefficient $\beta = 0.025$. The rail unevenness is characterized by its power spectral density $S_{u_{w/r}}(k_y)$ that decreases with the longitudinal wavenumber k_y as

$$S_{u_{w/r}}(k_y) = S_{u_{w/r}}(k_{y_0})(k_y/k_{y_0})^{-w}, \tag{3}$$

where $S_{u_{w/r}}(k_{y_0}) = 1.38 \times 10^{-8}\,\mathrm{m^3/rad}$, $k_{y_0} = 1\,\mathrm{rad/m}$ and $w = 3.5$ [9].

Fig. 3 shows the vertical component of the free field incident velocity computed in two points, P1 and P2, as indicated in Fig. 2. P1 is located on the soil's surface at a distance of 13 m from the central line of the track, while P2 lies 28 m from the track. The dominating part of the frequency content is between 20 and 80 Hz, but vibrations up to 150 Hz are also present in the incident wave field. The largest peaks around 50 Hz correspond to the resonance of the train's axles on the coupled track–soil system. The time history extends from −2 s until 2 s. The equidistant sharp peaks correspond to the 13 bogies of the train. Comparing the vibration levels in the two points, significant attenuation can be observed above 30 Hz, due to the geometrical and material damping in the soil.

3. The structural response

3.1. Methodology

A weak coupling between the incident wave field and the structure is assumed, meaning that the presence of the building has no effect on the vibration generation mechanism, and the free field displacements are applied as an excitation on the coupled soil–structure model.

The subdomain method proposed by Aubry et al. [10] and Clouteau [11] is used to formulate the dynamic soil–structure interaction problem. The displacement of the ground $\hat{\mathbf{u}}^g$ is written as a superposition of two displacement fields, $\hat{\mathbf{u}}_0$ and $\hat{\mathbf{u}}_{\mathrm{sc}}$, where $\hat{\mathbf{u}}_0$ is due to the incident wave field satisfying a zero displacement boundary condition on the soil–structure interface Σ, and $\hat{\mathbf{u}}_{\mathrm{sc}}$ is the displacement field radiated into the soil by the structural motion $\hat{\mathbf{u}}_b$ on the interface (Fig. 4).

The finite structure is modelled in the frequency domain by a 3D structural finite element method. The equation of motion of the building is

$$\left(\begin{bmatrix} \mathbf{K}_{ss} & \mathbf{K}_{sb} \\ \mathbf{K}_{bs} & \mathbf{K}_{bb} + \hat{\mathbf{K}}^g_{bb} \end{bmatrix} - \omega^2 \begin{bmatrix} \mathbf{M}_{ss} & \mathbf{M}_{sb} \\ \mathbf{M}_{bs} & \mathbf{M}_{bb} \end{bmatrix} \right) \begin{Bmatrix} \hat{\mathbf{u}}_s \\ \hat{\mathbf{u}}_b \end{Bmatrix} = \begin{Bmatrix} \mathbf{0} \\ \hat{\mathbf{f}}_b \end{Bmatrix}, \tag{4}$$

where the structural displacements $\hat{\mathbf{u}}^s$ are separated to the displacement dof of the foundation $\hat{\mathbf{u}}_b$ and the remaining dof of the superstructure $\hat{\mathbf{u}}_s$. $\mathbf{M}$ and $\mathbf{K}$ denote the finite element mass and stiffness matrices, and $\hat{\mathbf{K}}^g_{bb}$ stands for the frequency-dependent impedance matrix of the soil. The force $\hat{\mathbf{f}}_b$ is expressed as the total force due to the wave field $\hat{\mathbf{u}}_0$, acting on the clamped interface:

$$\hat{\mathbf{f}}_b = \int_\Sigma \mathbf{N}^{\mathrm{T}} \hat{\mathbf{t}}(\hat{\mathbf{u}}_0)\,\mathrm{d}\Sigma, \tag{5}$$

where $\hat{\mathbf{t}}(\hat{\mathbf{u}}_0)$ denotes the tractions on the interface due to the wave field $\hat{\mathbf{u}}_0$, and $\mathbf{N}$ denotes the shape functions.

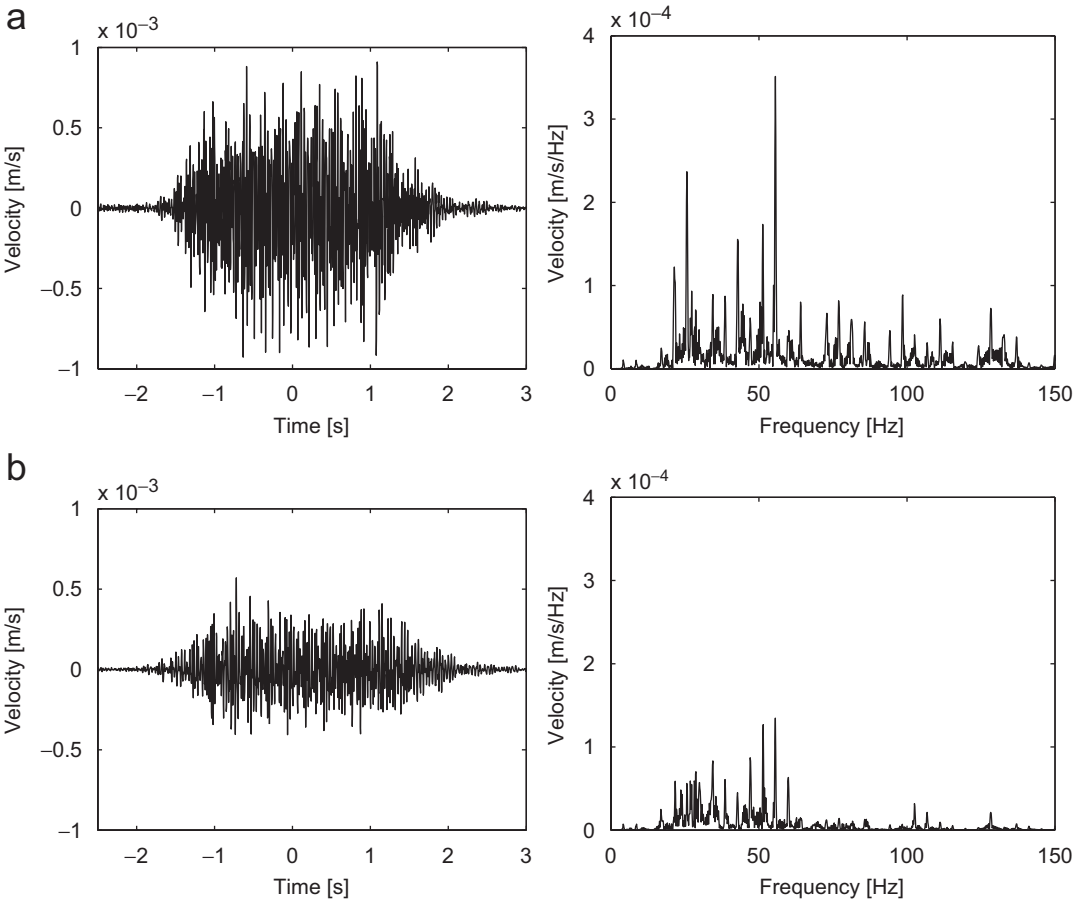

Fig. 3. Time history and frequency content of the free field vertical velocity in the points (a) P1 and (b) P2.

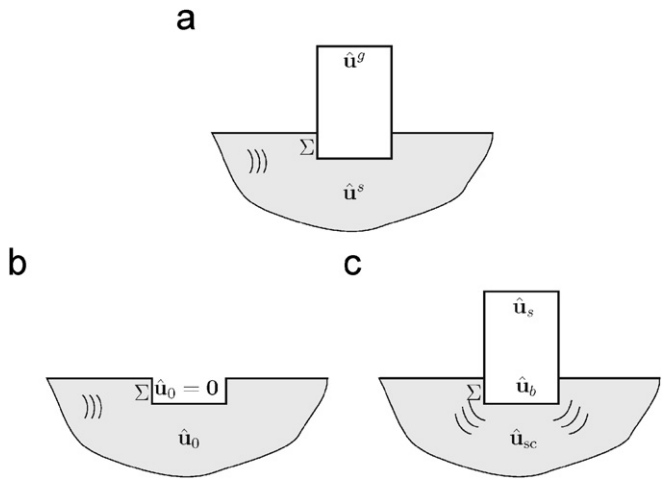

Fig. 4. The soil displacement field $\hat{\mathbf{u}}^g$ (a) is decomposed into (b) a displacement field $\hat{\mathbf{u}}_0$ and (c) a radiated field $\hat{\mathbf{u}}_{sc}$.

The soil tractions and the impedance of the soil are computed using a 3D boundary element method [11] in the frequency domain, using the Green's functions of a layered half-space [21].

A Craig–Bampton [22] modal decomposition method is used in order to reduce computational costs. The displacement vector of the foundation is written as a superposition of rigid and flexible foundation modes $\mathbf{\Phi}_b$, while the displacement vector of the superstructure is decomposed into the quasi-static transmission $\mathbf{\Phi}_b^s$ of the foundation modes to the superstructure and the flexible modes $\mathbf{\Phi}_s$ of the superstructure with a clamped base:

$$\begin{Bmatrix} \hat{\mathbf{u}}_s \\ \hat{\mathbf{u}}_b \end{Bmatrix} = \begin{bmatrix} \mathbf{\Phi}_s & \mathbf{\Phi}_b^s \\ \mathbf{0} & \mathbf{\Phi}_b \end{bmatrix} \begin{Bmatrix} \hat{\boldsymbol{\alpha}}_s \\ \hat{\boldsymbol{\alpha}}_b \end{Bmatrix}. \tag{6}$$

This substructuring method has the advantage that the foundation and the superstructure are decoupled. If modifications are made to the building's superstructure, the forces resulting from the incident wave field do not have to be recomputed.

3.2. The office building model

The finite element mesh of the portal frame structure is shown in Fig. 5. The building's dimensions are 15 m × 10 m × 9.6 m, and the distance between the track's central line and the nearest edge of the structure is 13 m.

The three story superstructure is supported by a 0.3 m thick reinforced concrete raft foundation. The basic structure consists of a reinforced concrete portal frame structure containing vertical columns of cross-sectional dimensions 0.3 × 0.3 m and horizontal beams of dimensions 0.3 × 0.2 m. This frame structure supports three 0.3 m thick horizontal slabs. The structure has a reinforced concrete central core which surrounds the staircase. The thickness of the core walls is 0.15 m. The structural model is extended with the in-fill walls of three rooms besides the core. Room 1 has dimensions 5 × 6 × 3 m, and is located in the first floor, behind the core wall; room 2, which has the same dimensions, is located on the second floor; a smaller room 3 with dimensions 5 × 4 × 3 m is located on the first floor, besides the core. The masonry in-fill walls are 0.06 m thick.

The finite element size is chosen as 0.25 m, which is fine enough for computations up to 150 Hz. The total model has 85 518 degrees of freedom. A constant hysteretic structural damping of $\beta_s = 0.025$ is assumed.

3.3. The modes of the structure

According to the Rubin criterion [23], all the modes up to 1.5 × 150 Hz have to be taken into account in the modal superposition in order to have a kinematic base that is sufficient up to a frequency of 150 Hz. In the present study, all the foundation and superstructure modes up to 300 Hz have been accounted for. A few modes are displayed in Fig. 6. The lowest mode of the superstructure with a clamped base is at 2.60 Hz, and

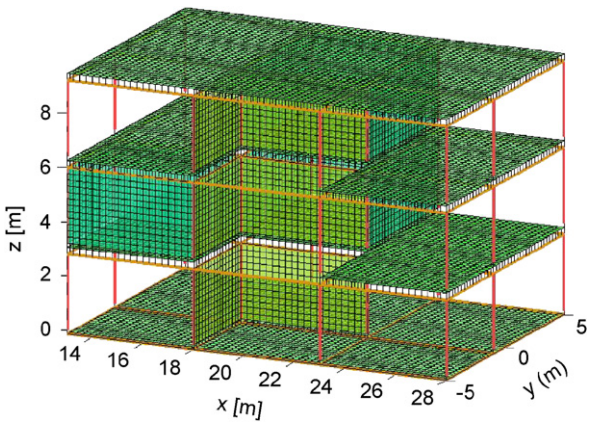

Fig. 5. Finite element mesh of the office building.

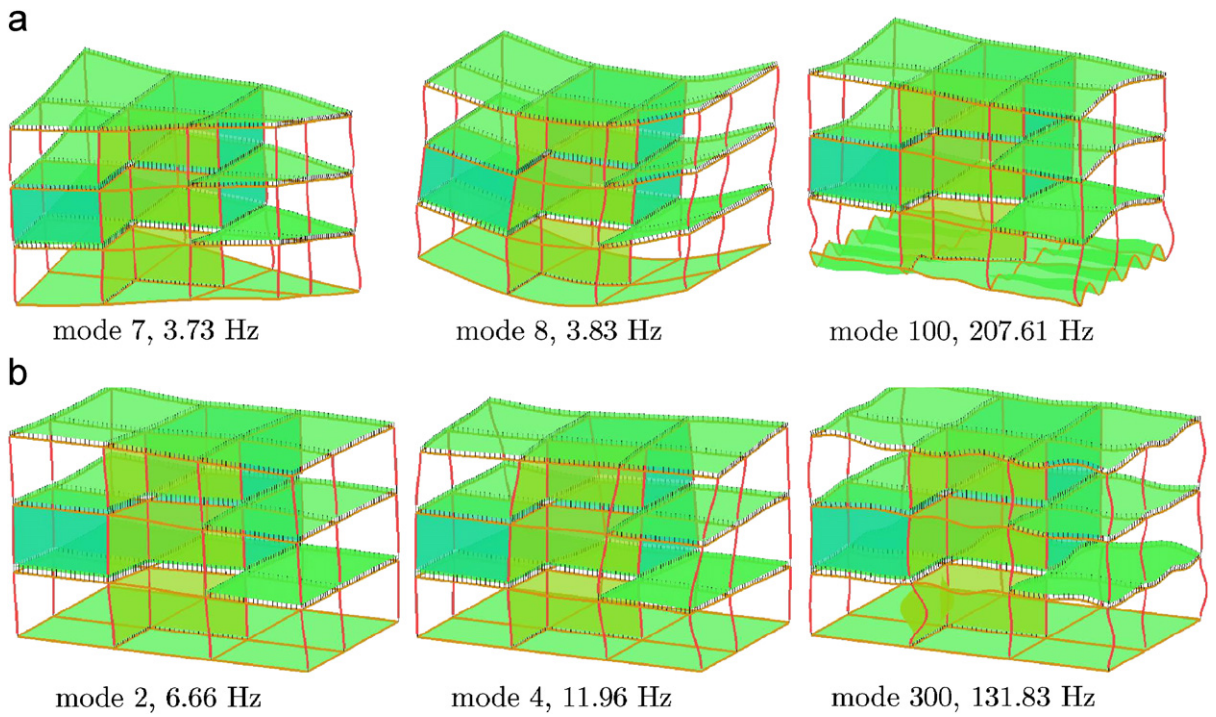

Fig. 6. (a) Quasi-static transmission of flexible foundation modes on the superstructure and (b) flexible modes of the superstructure with clamped foundation.

only 12 modes of the superstructure have been found under 20 Hz. These low-frequency modes are the global torsional and bending modes of the whole building. Above 50 Hz, however, the modal density tends to be very high and the high-frequency modal shapes show local bending modes of the floor slabs and the core walls. For this particular case, the modal density of the foundation and the superstructure is close to constant in the higher frequency range. The total number of superstructure and foundation modes that is accounted for is equal to 829 and 203, respectively.

3.4. The impedance of the soil

For the computation of the soil's impedance, the same foundation mesh as introduced in Fig. 5 has been used in a boundary element method based on the Green's functions of a layered half-space. Figs. 7 and 8 show the real and imaginary part $k(\omega)$ and $c(\omega)$ of the soil's impedance $K^g(\omega) = k(\omega) + i\omega c(\omega)$ corresponding to a horizontal and the vertical rigid body displacement of the foundation. The functions show that the real part decreases slowly, while the imaginary part increases with frequency in the higher frequency domain. This means that, at higher frequencies, the radiation damping dominates the soil's impedance.

3.5. Structural response

In the following, the structural response of the office building to the passage of the high-speed train is presented. Different modelling options are considered with respect to the effect of dynamic soil–structure interaction.

First, it is assumed that dynamic soil–structure interaction does not have a significant effect on the ground borne structural vibrations and re-radiated noise. This assumption is very attractive from a computational point of view, because the determination of the soil's impedance with a 3D boundary element method can be

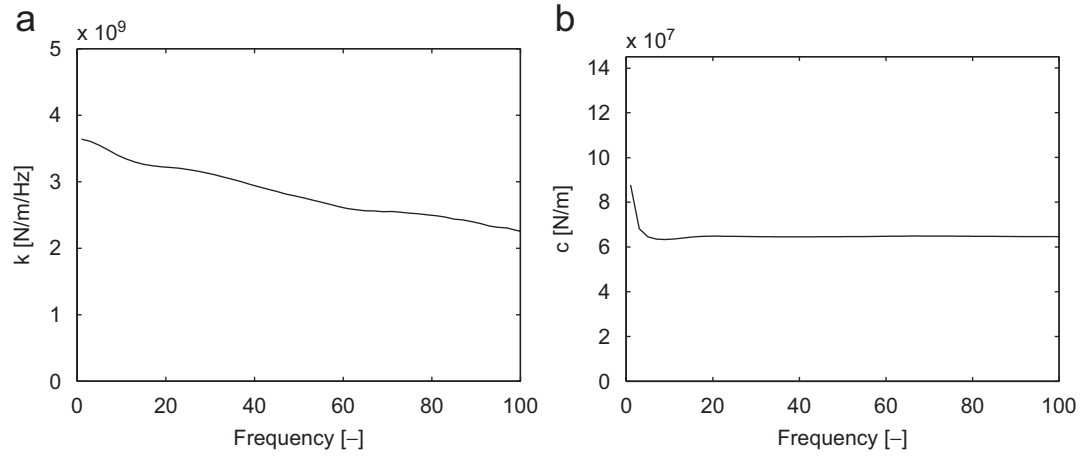

Fig. 7. (a) Real and (b) imaginary part of the soil's impedance corresponding to the horizontal (x) rigid body mode of the foundation.

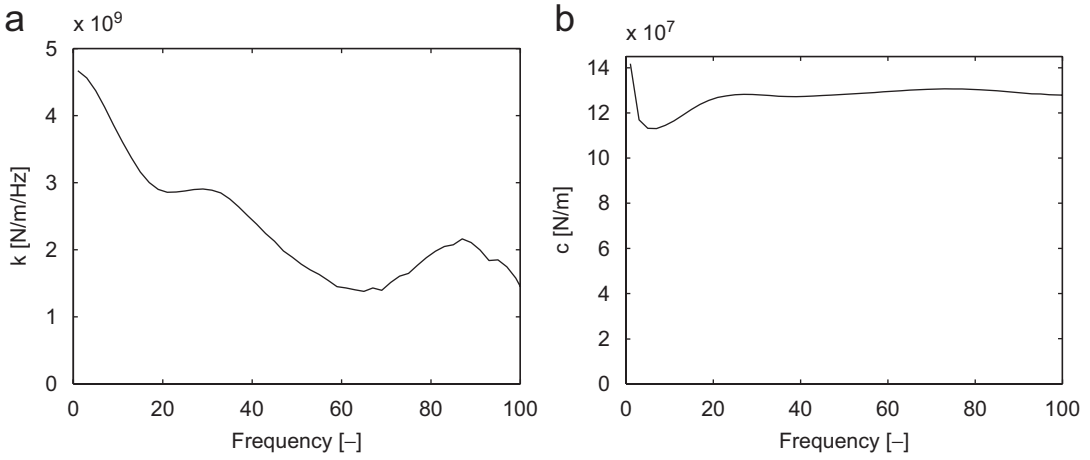

Fig. 8. (a) Real and (b) imaginary part of the soil's impedance corresponding to the vertical rigid body mode of the foundation.

avoided. Some assumptions have to be made, however, regarding the impedance difference between the soil and the foundation.

If the soil is much stiffer than the structure, it can be assumed that the incident wave field is not affected by the structure, and the structure's foundation can be directly excited with the incident soil displacements. The modal coordinates $\boldsymbol{\alpha}_b$ of the foundation can be obtained by a least mean squares approximation of the incident wave field, using a superposition of the rigid and flexible foundation modes $\boldsymbol{\Phi}_b$:

$$\boldsymbol{\alpha}_b = [\boldsymbol{\Phi}_b^{\mathrm{T}}\boldsymbol{\Phi}_b]^{-1}\boldsymbol{\Phi}_b^{\mathrm{T}}\mathbf{u}_{\mathrm{inc}}. \tag{7}$$

If the structure is much stiffer than the soil, it can be assumed that only rigid body modes of the foundation are excited by the incident wave field. The modal coordinates $\boldsymbol{\alpha}_b$ can be determined by using Eq. (7) where only the six rigid body foundation modes are incorporated in $\boldsymbol{\Phi}_b$.

In the third modelling case, dynamic soil–structure interaction is accounted for with the assumption of a flexible foundation. The soil's impedance and the loading forces are computed with the boundary element method and Eq. (4) is solved.

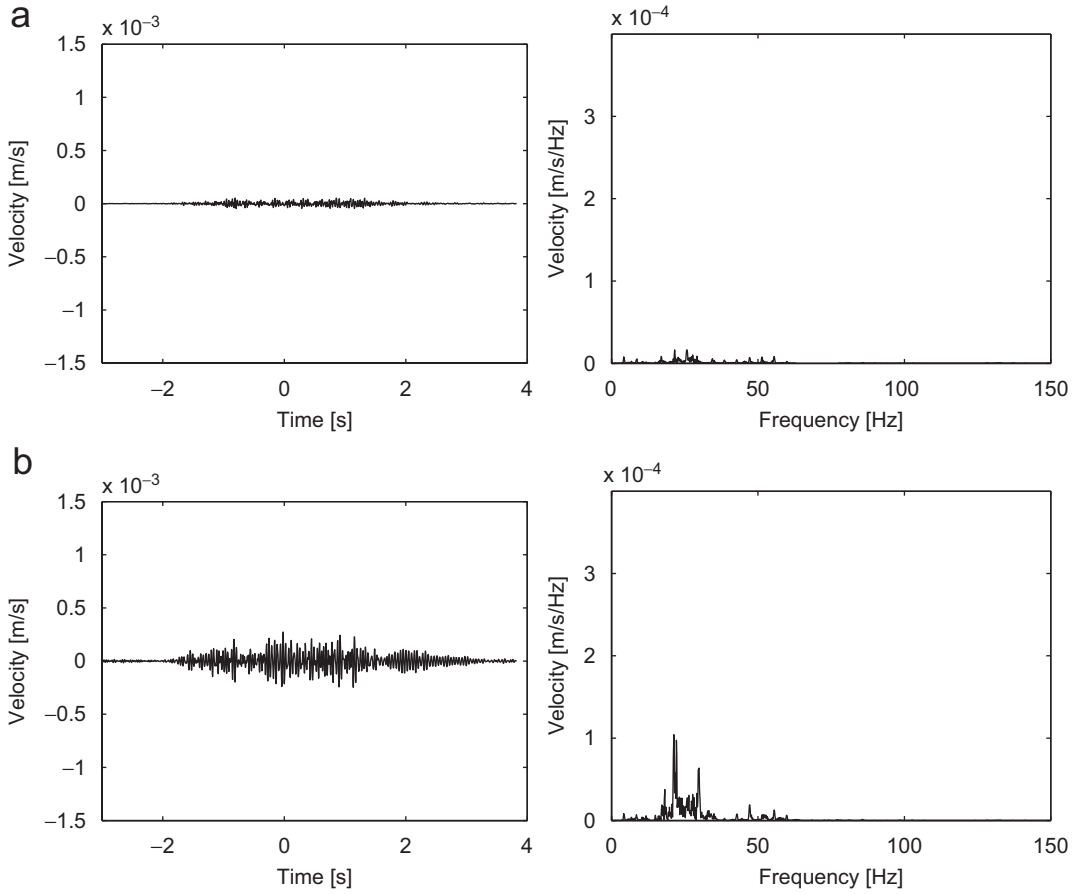

Fig. 9. Time history and frequency content of the vertical velocity in the points Q1 (a) and Q2 (b) for the case of a rigid foundation without dynamic soil–structure interaction taken into account.

Figs. 9–11 display the vertical velocity in two points Q1 and Q2 of the building for the three modelling cases. The point Q1 is located on the ground level and Q2 is located on the floor of room 1, both at horizontal coordinates $x = 20.5\,\mathrm{m}$ and $y = 2\,\mathrm{m}$.

For the case of the rigid foundation without dynamic soil–structure interaction (Fig. 9), only very small vertical vibration levels are observed on the foundation (point Q1). This is due to the fact that the rigid body motion of the foundation results in a suppression of the horizontally propagating ground vibrations above 20 Hz, as their wavelength is smaller than the foundation's dimension in the x direction. However, a significant vibration amplification can be observed between the foundation (point Q1) and the first floor (point Q2) due to the first local bending modes of the floor slab in the frequency range between 20 and 30 Hz.

As the dominant frequency range of soil vibrations is above 20 Hz, the assumption of a flexible foundation results in much larger vibration levels on the foundation (Figs. 10 and 11). The vertical vibrations are strongly amplified at the local bending modes of the slabs at the first floor. The ground vibrations above 50 Hz are not transmitted up to the first floor, which is an effect of structural damping. Comparing Figs. 10 and 11, the effect of dynamic soil–structure interaction on the structure with a flexible foundation can be investigated. As the soil is rather stiff, the vibration levels are similar for both cases. Soil–structure interaction results in an attenuation of the incident wave field in the higher frequency range (above 50 Hz). It can be concluded that, in the present case, the effect of dynamic soil–structure interaction can be disregarded in good approximation, if the imposed wave field on the structure incorporating the flexible foundation is properly represented, according to Eq. (7).

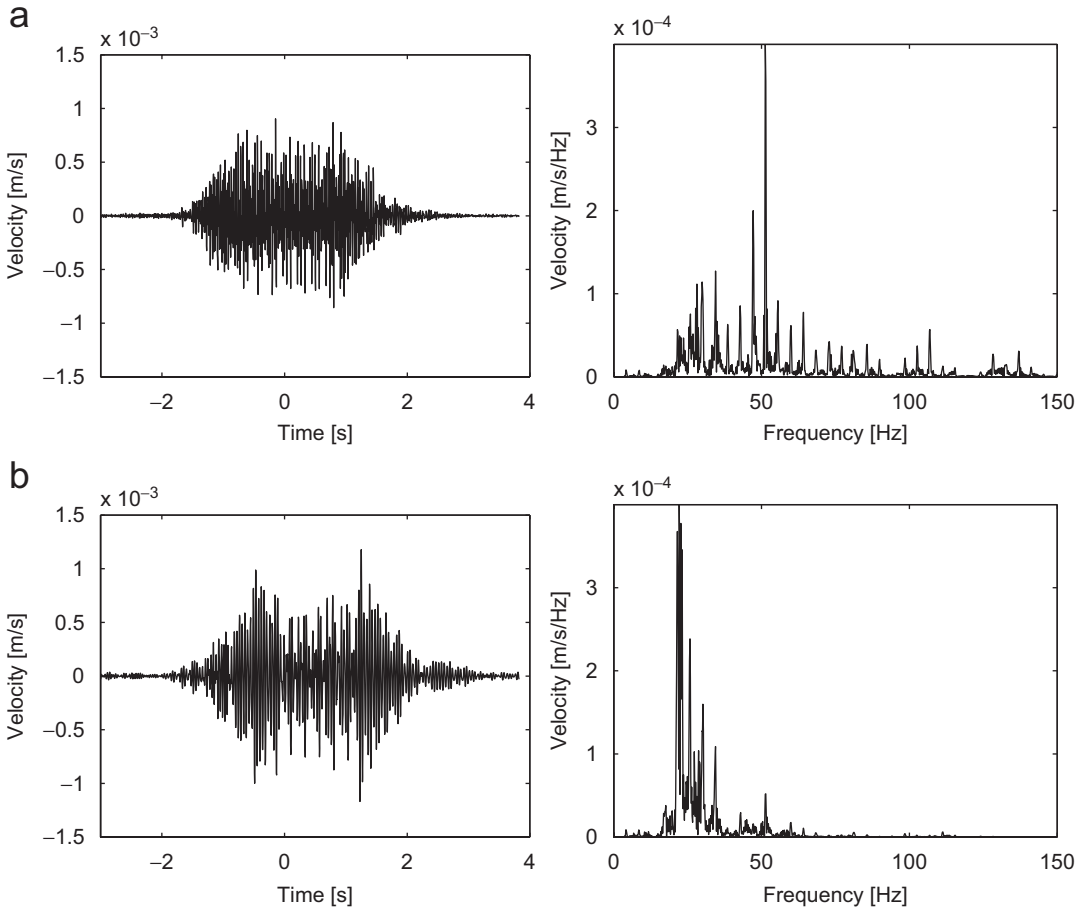

Fig. 10. Time history and frequency content of the vertical velocity in the points Q1 (a) and Q2 (b) for the case of a flexible foundation without dynamic soil–structure interaction taken into account.

4. Acoustic response

4.1. Methodology

After determining the structural response of the building, the acoustic radiation problem can be now solved. As the impedance of the radiating walls is much larger than that of the internal acoustic space, a weak coupling between structural and acoustic vibrations is assumed. The acoustic pressure inside the room has no effect on the vibration of the walls and the computed structural vibration velocity is applied as a boundary condition in an acoustic boundary value problem.

The internal acoustic space is characterized by the speed of sound C_a and the material density of the air ρ_a. The absorbing surfaces of the rooms are characterized by the acoustic impedance Z_a, relating the acoustic pressure p_a to the difference of normal structural and acoustic velocities $\hat{v}_s$ and $\hat{v}_a$ of the acoustic boundary Γ_a:

$$\hat{p} = Z_a(\hat{v}_s - \hat{v}_a). \tag{8}$$

At relative low frequencies, the acoustic impedance can be computed from the walls' acoustic absorption coefficient α, which gives the ratio of the absorbed and the incident acoustic energy when a normal incident acoustic plane wave is reflected from the surface. The relation between the acoustic absorption coefficient and

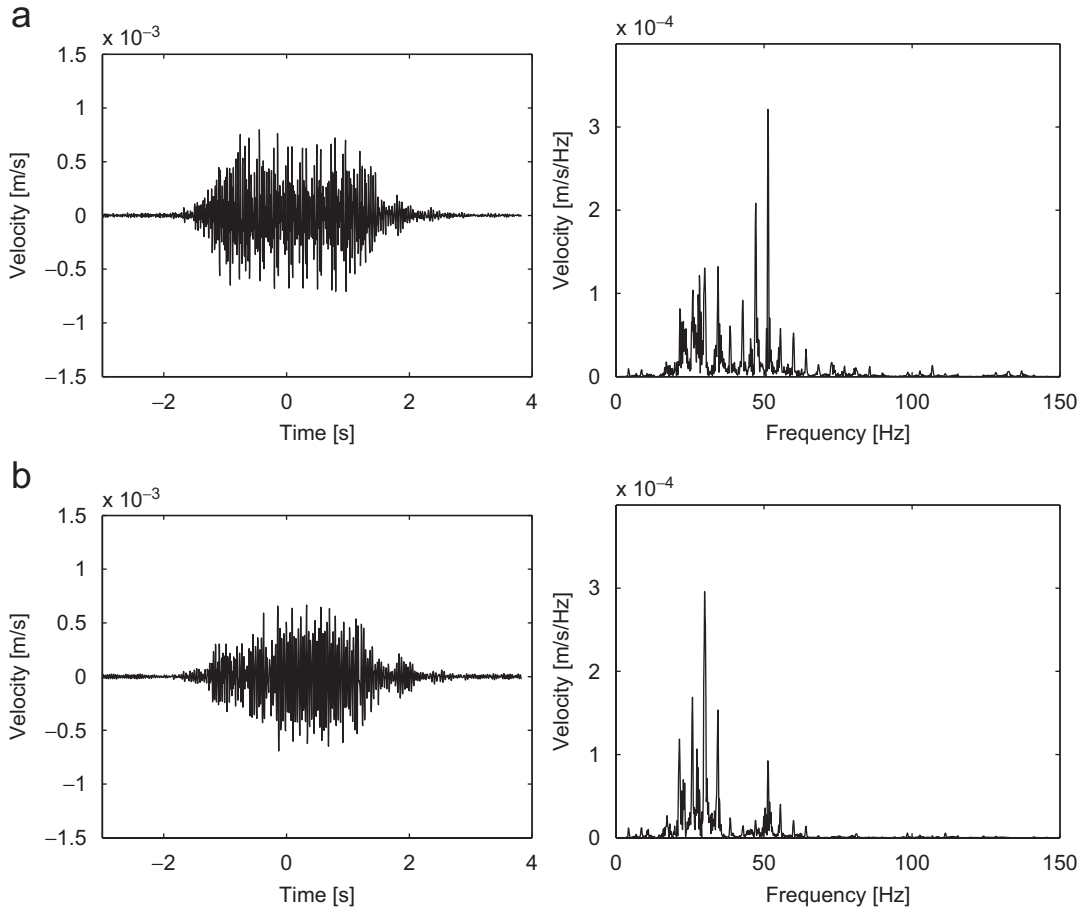

Fig. 11. Time history and frequency content of the vertical velocity in the points Q1 (a) and Q2 (b) for the case of a flexible foundation with dynamic soil–structure interaction taken into account.

the wall's impedance can be approximated as

$$Z_a = \rho_a C_a \frac{1+\sqrt{1-\alpha}}{1-\sqrt{1-\alpha}}. \tag{9}$$

An acoustic spectral finite element method [24], is used to express the internal pressure $\hat{p}_a(\mathbf{x},\omega)$ in terms of the acoustic room modes:

$$\hat{p}_a(\mathbf{x},\omega) = \sum_n \Psi_n(\mathbf{x})\hat{\beta}_n(\omega), \tag{10}$$

where $\Psi_n(\mathbf{x})$ denotes the nth acoustic mode of the shoe-box shaped interior domain with rigid boundary conditions and $\hat{\beta}_n(\omega)$ is the corresponding modal coordinate.

The application of the spectral finite element method results in a system of linear equations for the acoustic modal coordinates $\hat{\beta}_n$:

$$(\mathbf{\Lambda} + \mathrm{i}\omega\mathbf{D} - \omega^2\mathbf{I})\hat{\boldsymbol{\beta}} = \mathrm{i}\omega\hat{\mathbf{F}}, \tag{11}$$

where $\mathbf{\Lambda} = \mathrm{diag}\{\omega_n^2\}$ contains the eigenfrequencies of the acoustic domain, $\mathbf{I}$ is a unit matrix, $\mathbf{D}$ denotes the modal damping matrix related to the wall absorption, and $\hat{\mathbf{F}}$ denotes the modal load vector. The elements of

the **D** matrix are defined by

$$D_{nm} = \rho_a C_a^2 \int_{\Gamma_a} \frac{\Psi_n \Psi_m}{Z_a} \mathrm{d}\Gamma, \tag{12}$$

where n and m are the column and row indices, respectively, and the nth element of the **F** vector is given by

$$\hat{F}_n = \rho_a C_a^2 \int_{\Gamma_a} \Psi_n \hat{v}_s \, \mathrm{d}\Gamma. \tag{13}$$

For the case of constant wall absorption on the boundary, the values D_{nm} can be expressed analytically. Moreover, the off-diagonal elements can be truncated with a relative small error [25], resulting in a very fast algorithm for the acoustic computations. In this case the spectral finite element method results in a direct boundary integral representation of the acoustic modal coordinates.

4.2. Acoustic properties

The dimensions of room 1 and room 2 are 5 m × 6 m × 2.8 m, while the size of room 3 is 5 m × 4 m × 2.8 m. The sound velocity is equal to $C_a = 343\,\mathrm{m/s}$ and the density of the air is $\rho_a = 1.225\,\mathrm{kg/m^3}$. The absorption is assumed to be constant on the rooms' surface and over the whole frequency range. Two different absorption coefficients are considered for the three rooms: $\alpha = 0.03$ for a strongly reflecting room with uncovered concrete walls and an uncarpeted floor, and $\alpha = 0.15$ is typical for an unfurnished, carpeted room [26,27]. Using Sabine's formula [28], the reverberation time t_{rev} can be approximated from the room's volume V, the surface area A and the average absorption coefficient α as

$$t_{\mathrm{rev}} = \gamma \frac{V}{\alpha A}, \tag{14}$$

where $\gamma = 0.16\,\mathrm{s/m}$. For the case of the larger rooms (room 1 and room 2), the absorption coefficients $\alpha = 0.03$ and 0.15 result in reverberation times of 3.3 and 0.66 s, respectively, while for the case of the smaller room 3 these reverberation times are 3.68 and 0.73 s.

4.3. Acoustic modes

The acoustic modes of a rectangular domain are characterized by the number of half wavelengths (n_x, n_y, n_z) along the three room dimensions. The mode (2, 3, 1) of room 3 at 158 Hz is plotted in Fig. 12. A modal base including all the acoustic modes up to 400 Hz has been used for the spectral finite element method.

The computational effort of the structural and acoustic computations is determined by the number of modes taken into account in the modal superposition. Fig. 13 shows the number of structural and acoustic modes as a function of upper frequency limit, i.e. the total number of modes between 0 Hz and the given frequency value. In the lower frequency range, the structural modal density is much higher than the acoustic.

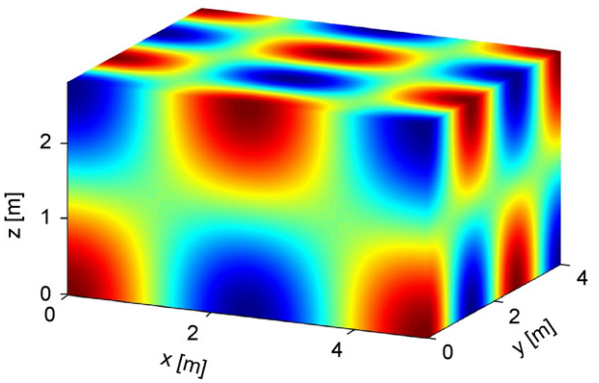

Fig. 12. Acoustic mode (2, 3, 1) of room 3 at 158 Hz.

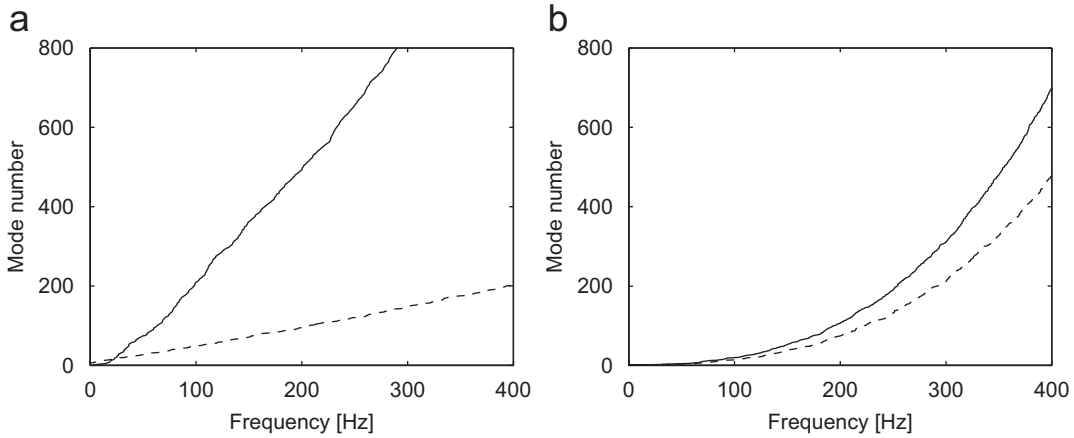

Fig. 13. Number of (a) structural modes as a function of the upper frequency limit for the foundation (dashed line) and the superstructure (solid line) and (b) number of acoustic modes for room 1 (solid line) and room 3 (dashed line).

Table 1
Mode numbers and frequencies of the first acoustic modes of room 1

f (Hz)	n_x	n_y	n_z
28.58	0	1	0
34.30	1	0	0
44.64	1	1	0
57.16	0	2	0
61.25	0	0	1
66.66	1	2	0
67.59	0	1	1
68.60	2	0	0
70.20	1	0	1

Table 2
Mode numbers and frequencies of the first acoustic modes of room 3

f (Hz)	n_x	n_y	n_z
34.30	1	0	0
42.87	0	1	0
54.90	1	1	0
61.25	0	0	1
68.60	2	0	0
70.20	1	0	1
74.76	0	1	1
80.90	2	1	0
82.25	1	1	1

However, the structural modal density shows a slight variation with frequency while the acoustic modal density increases more rapidly. With an upper frequency limit of 200 Hz, the computational times for determining the structural response and the acoustic response in a single room are of the same order of magnitude.

Referring to the frequency range of structural vibrations on the first floor, it is clear that the dominant frequencies of the acoustic response will be determined by the first few acoustic modes. The eigenfrequencies and modal numbers of these modes are listed in Tables 1 and 2.

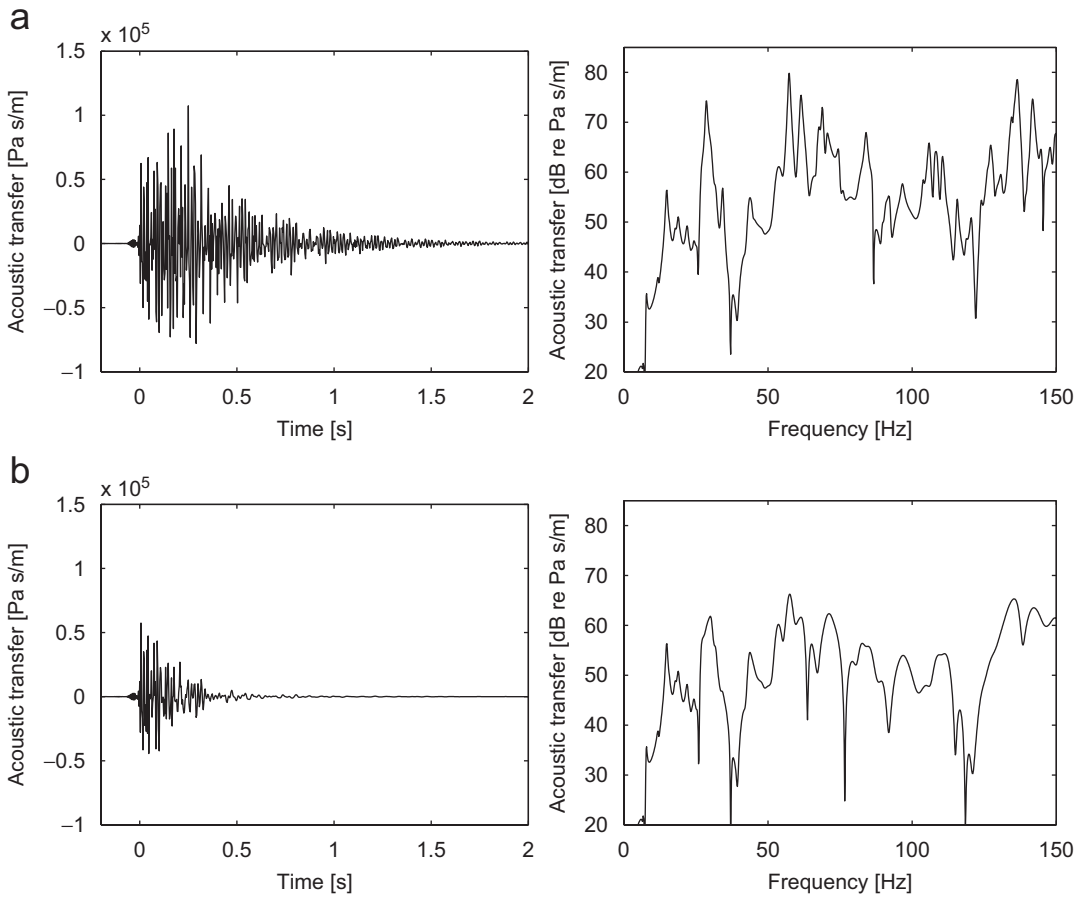

Fig. 14. Transfer function between the vertical velocity of the rigid foundation and the sound pressure in room 1 for (a) $\alpha = 0.03$ and (b) $\alpha = 0.15$.

4.4. Transfer functions

In the following, transfer functions are presented which relate the sound pressure in an internal point of room 1 to the vertical rigid body motion of the foundation. The point Q3 is located at $x = 20\,\text{m}$, $y = 1.4\,\text{m}$, $z = 4.32\,\text{m}$, slightly shifted from the centre of room 1 in order to find the contribution of as many modes as possible.

Fig. 14 shows the transfer functions in the time and the frequency domain, for the case of both absorption coefficients. These transfer functions can be used to give an estimate of the noise caused by the ground borne vibration, if the velocity of the incident wave field is known. The frequency domain functions show a constant trend above 50 Hz. This implies that the dominant frequency range of re-radiated sound does not differ from the frequency range of the incident velocity. The first sharp peak in the frequency content appears around 30 Hz. At this frequency, the first bending modes of the room's walls excite the first horizontal acoustic modes of the room. The maximum level of the frequency content is at the first vertical acoustic resonance. Above this frequency, a lot of very sharp peaks are found corresponding to lower absorption. For the case of $\alpha = 0.15$, these peaks are damped by approximately 10 dB. Time histories of the transfer function are obtained by applying an inverse FFT and reveal good correspondence with the reverberation times predicted by Sabine's formula.

4.5. Acoustic response to high-speed train excitation

Fig. 15 displays the time history and the one-third octave band spectra of the sound pressure in room 1, induced by the passage of the high-speed train. The figure shows the response for the lower absorption

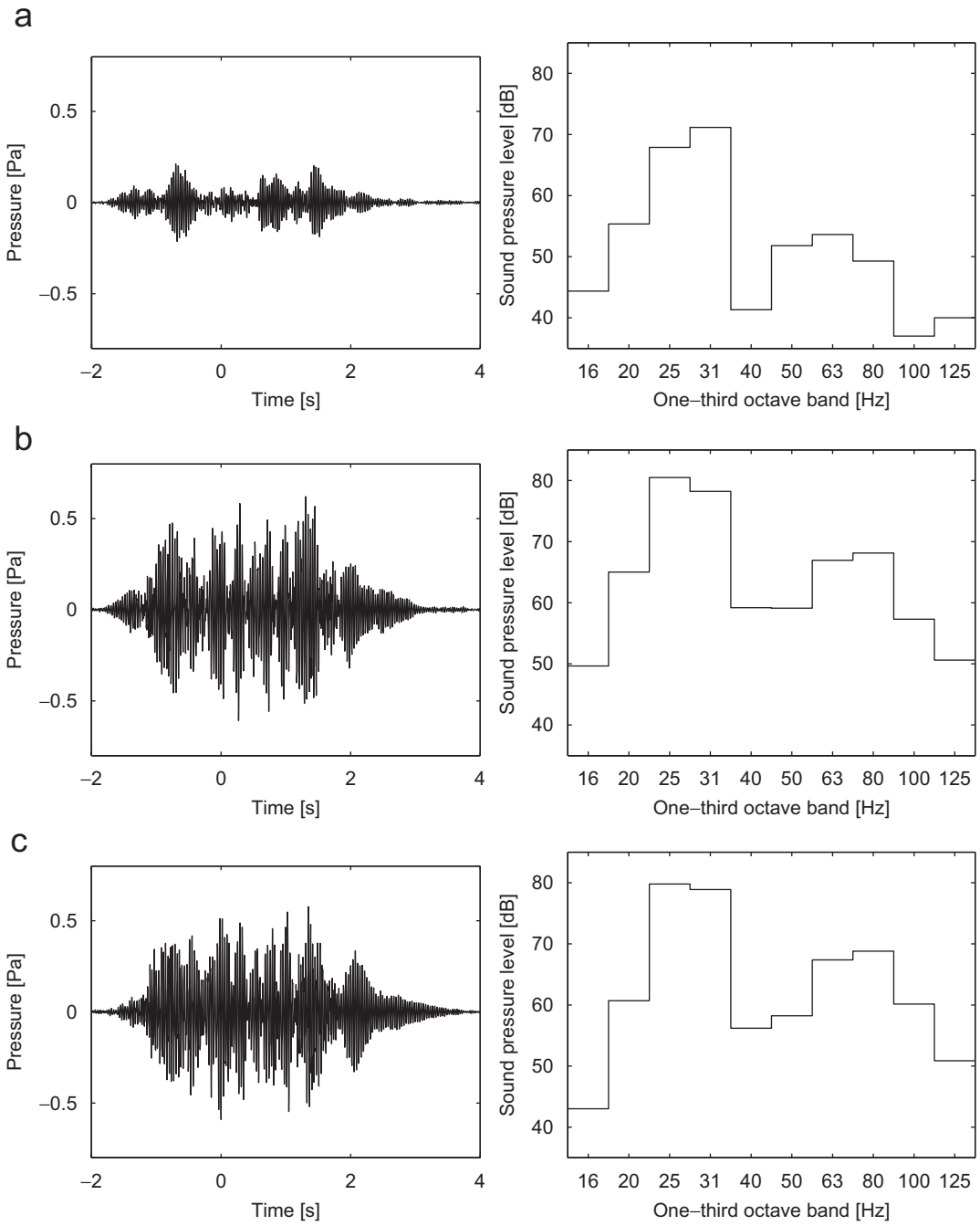

Fig. 15. Time history and one-third octave band levels of the sound pressure in room 1 during the passage of a HST for the case of $\alpha = 0.03$ and for (a) a rigid foundation without dynamic SSI, (b) a flexible foundation without dynamic SSI and (c) a flexible foundation with dynamic SSI.

coefficients $\alpha = 0.03$, and for all the three modelling cases. For the case of the rigid foundation without dynamic soil–structure interaction, only the first horizontal acoustic modes are excited, resulting in a sound pressure level of 70 dB in the 25 and 31 Hz bands. For the case of the flexible foundation, the dominant one-third octave bands are those containing the room's resonance frequencies at 28.6 Hz (mode (1,0,0)), 34.3 Hz

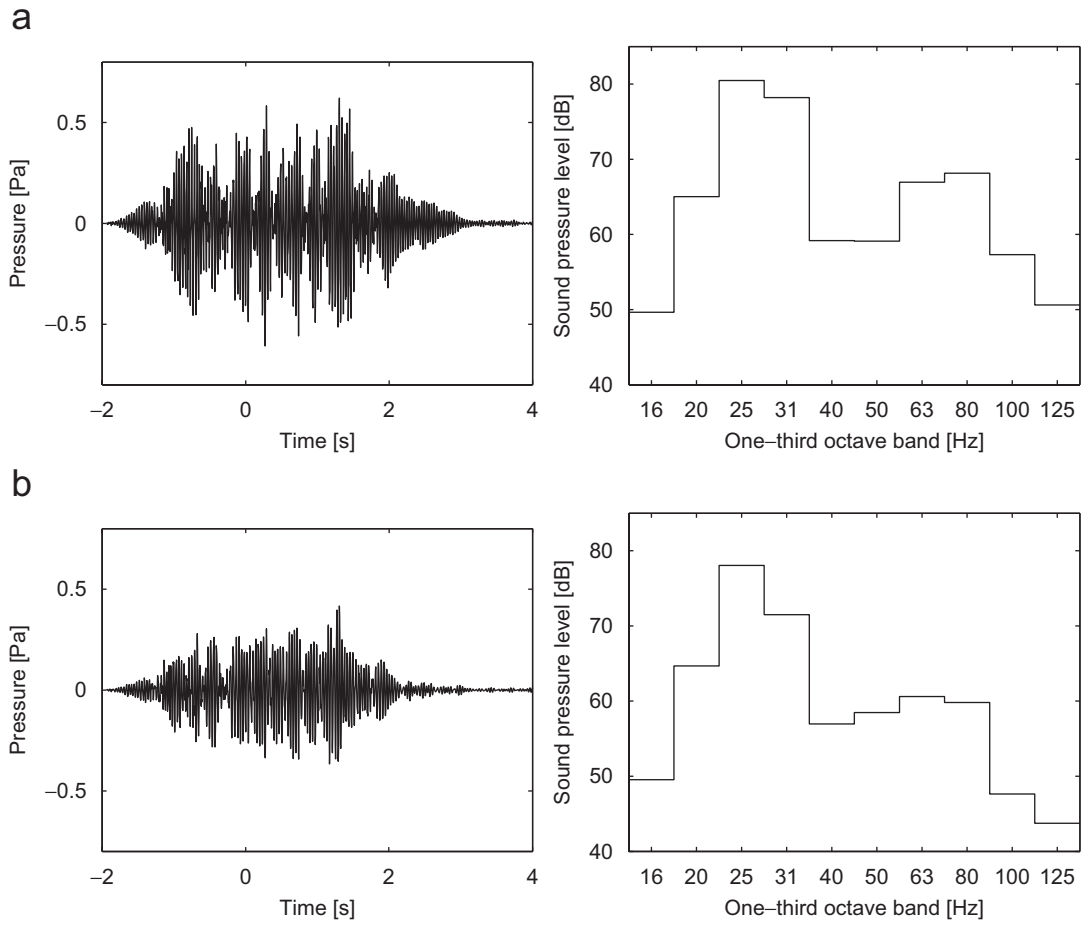

Fig. 16. Time history and one-third octave band levels of the sound pressure in room 1 during the passage of the high-speed train for the case of a flexible foundation without dynamic SSI, with (a) $\alpha = 0.03$ and (b) $\alpha = 0.15$.

(mode (0,1,0)), 57.2 Hz (mode (2,0,0)), 61.25 Hz (mode (0,0,1)) and 68.6 Hz (mode (0,2,0)). The maximum level is found in the 25 Hz band. Due to the frequency-dependent sensitivity of the human ear, the observed noise is determined by the 63 and 80 Hz band peaks. Comparing Figs. 15b and c, it can be found that dynamic soil–structure interaction has a negligible effect on the re-radiated noise.

Fig. 16 shows the sound pressure in room 1 to the passage of the high-speed train for the two absorption coefficients. The one-third octave band spectra show a difference of 5 dB between the two wall absorptions above the first acoustic resonance of the room. In the time histories, the difference in reverberation time is clearly visible.

4.6. *Response to high-speed train excitation in different rooms of the building*

The sound pressure levels in the three rooms due to the passage of the high-speed train are compared in Fig. 17 for the case where dynamic soil–structure interaction is not accounted for and the foundation is assumed to be flexible. Comparing the pressure levels in rooms 1 and 2 that are of the same dimensions but at different levels of the building, a slight amplification at the first two horizontal modes can be observed. Fig. 17c corresponds to room 3 that is on the first story but has different dimensions than room 1. As the first

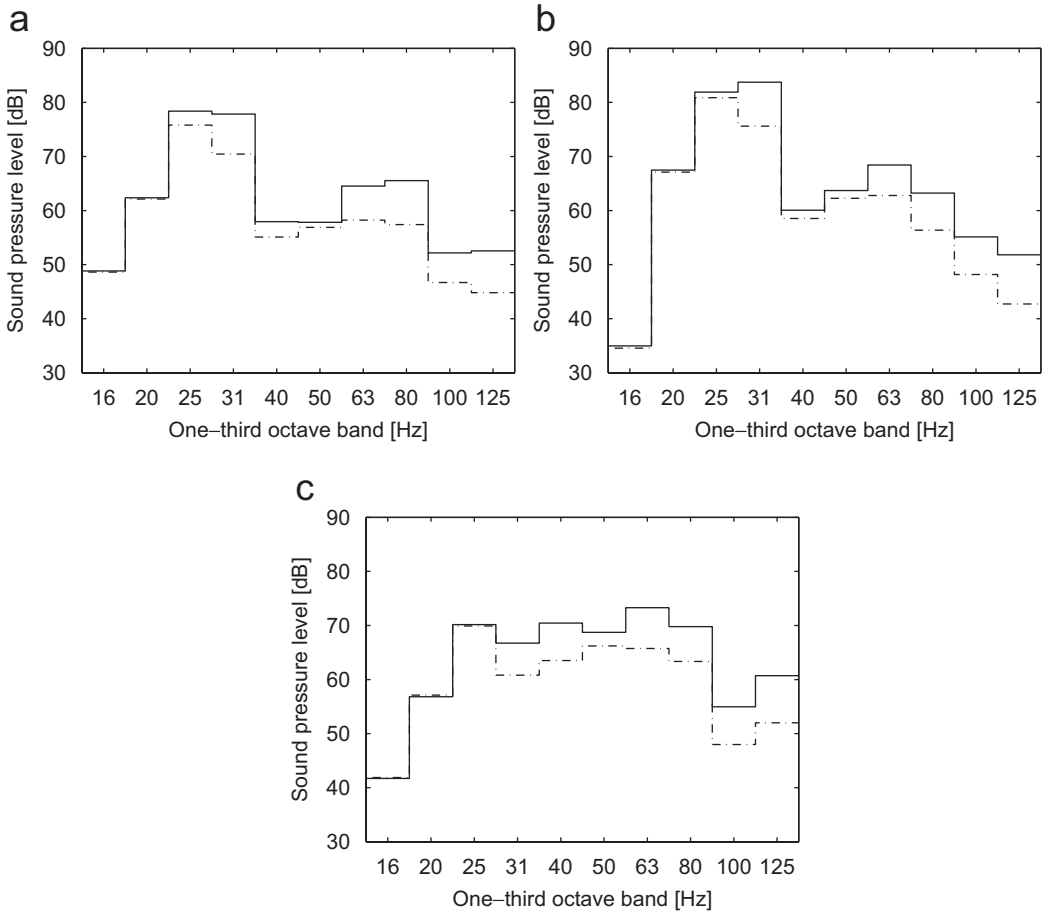

Fig. 17. One-third octave band spectra of the sound pressure in (a) room 1, (b) room 2 and (c) room 3 to the passage of the high-speed train for the case of $\alpha = 0.03$ (solid line) and $\alpha = 0.15$ (dash–dotted line).

eigenfrequencies of this room (at 34.3, 42.85 and 61.3 Hz) are distributed uniformly in the frequency scale, the one-third octave band spectra are balanced between 25 and 80 Hz.

4.7. Vibration and noise isolation

The described methodology has been used to investigate the effectiveness of vibration and noise isolation methods. The first method is the insertion of a floating floor in the room (Fig. 18a) in order to isolate the vibrations of the floor slab from the room's interior floor. The second method, widely used in acoustic laboratories for both vibration and noise reduction purposes, is a box-within-box arrangement, where the whole interior boundary is isolated from the vibrations of the building's walls and slabs (Fig. 18b). The third, most practical application is the base isolation of the building, where the superstructure is isolated from the foundation by springs placed under the columns and the core walls on the basement level.

For the case of the floating floor, a concrete floor supported by discrete springs and isolated from the walls by resilient material has been investigated. The 10 cm wide concrete slab is modelled by 4-node shell elements. The springs are placed at a distance of 1 m from each other. Their stiffness has been determined so that the total stiffness of the support and the mass of the concrete slab result in a vertical resonance frequency of 10 Hz. The elastic material that horizontally isolates the floating floor from the walls has been modelled by springs chosen to give a horizontal resonance frequency of 8 Hz.

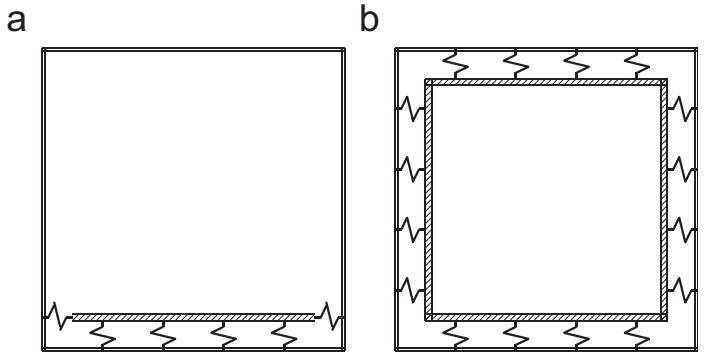

Fig. 18. Vibration and noise isolation of the room's interior by means of (a) a floating floor and (b) a box-within-box arrangement.

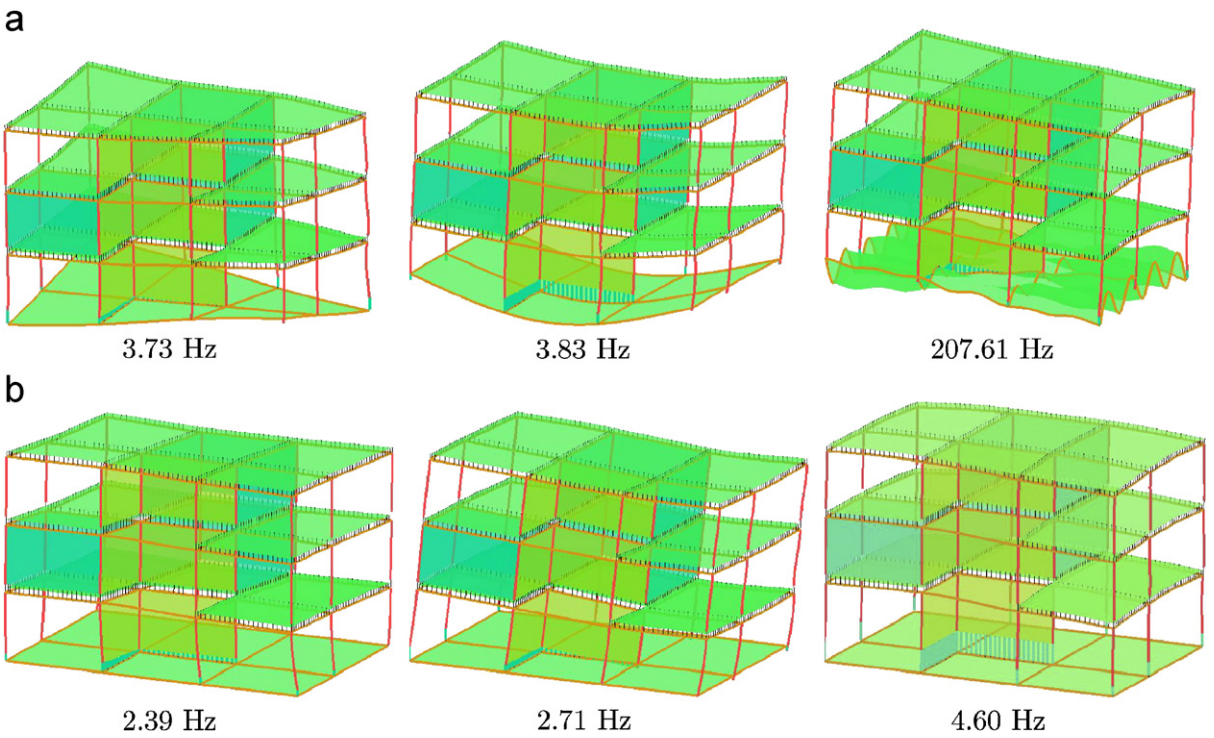

Fig. 19. (a) Quasi-static transmission of flexible foundation modes on the base-isolated superstructure and (b) flexible modes of the base-isolated superstructure with clamped foundation.

For the case of the box-within-box arrangement, the internal box consists of a 10 cm wide concrete floor slab and 6 cm wide concrete walls isolated by a resilient material. For the sake of simplicity, this material is modelled by a continuous spring–damper system, where the springs are connected to each node of the shell elements representing the floor and the walls. Similarly, the ceiling is modelled as a 6 cm thick wooden slab and a resilient material. Just as for the floating floor, the vertical and horizontal resonance frequencies have been chosen to 10 and 8 Hz, respectively.

For the case of the base-isolated building, 9 springs of equal stiffness k_z have been inserted below the structure's columns which are separated from the central core, and a distributed spring of total stiffness $3k_z$ has been inserted under the core. The stiffness k_z has been determined so that the vertical resonance frequency of the building on the springs is equal to 5 Hz.

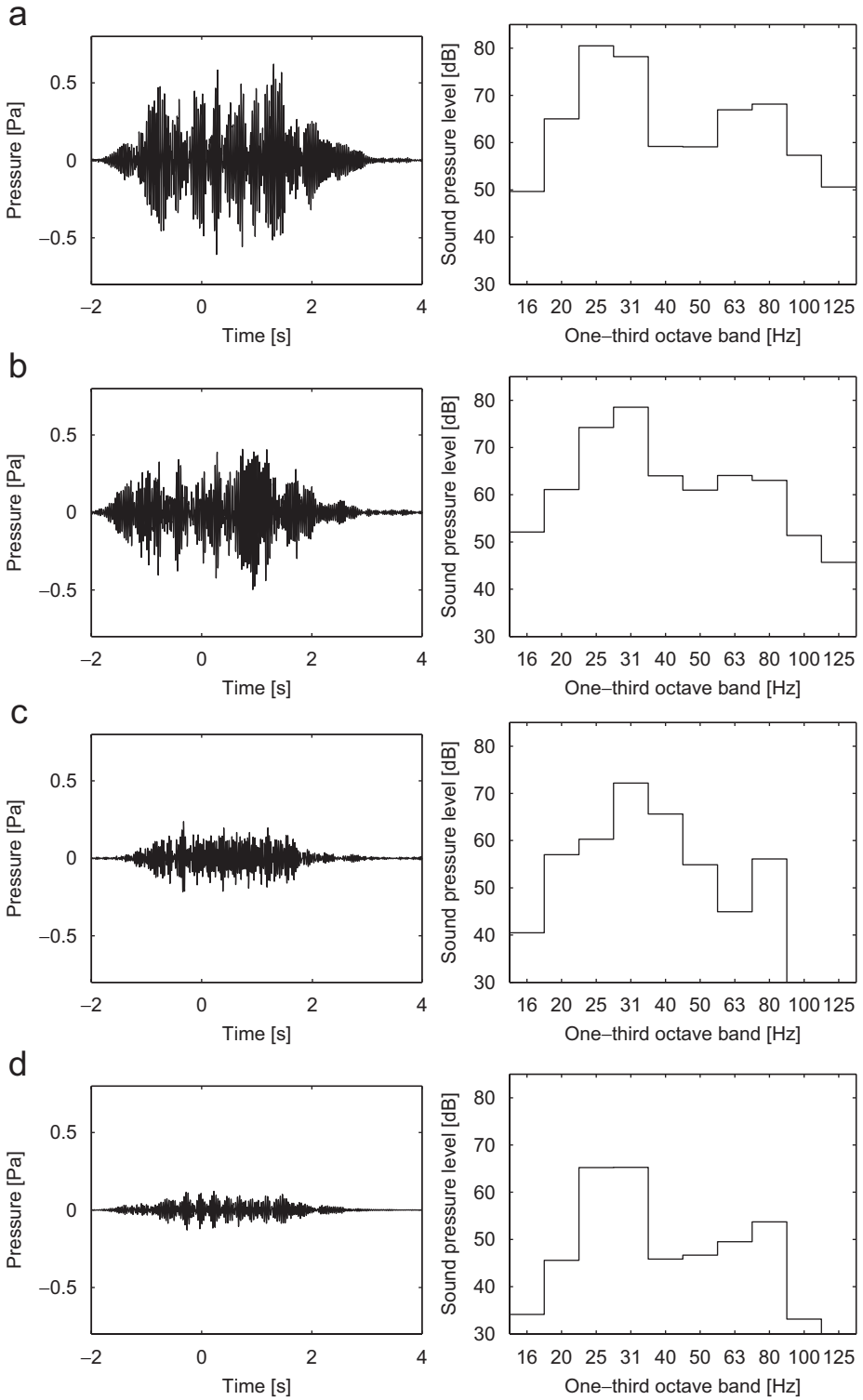

Fig. 20. Time history and one-third octave band spectra of the sound pressure in room 1 during the passage of a HST for the case of $\alpha = 0.03$ and (a) no vibration isolation, (b) a floating floor, (c) a box-within-box arrangement and (d) base isolation.

As the office superstructure is modified, the superstructure modes and the quasi-static transmission of the foundation modes have been recomputed. Fig. 19 shows some modes of the base-isolated structure. Fig. 19a shows the quasi-static transmission of the foundation modes, resulting in smaller modal displacements of the superstructure, due to the base isolation. Fig. 19b shows some low frequency modes of the base-isolated superstructure on a clamped foundation. These modes show rigid body motions of the original superstructure on the springs. Although the vertical resonance of the structure has been planned to 5 Hz, the actual resonance frequency of 4.60 Hz is somewhat lower, because the superstructure does not behave as a perfectly rigid body.

For the case of the floating floor and the box-within-box arrangement, where the internal volume of the acoustic space is modified, the acoustic computations have to be performed with the new modal base. However, as the Craig–Bampton method is used, the expensive computation of the soil's impedance and the forces does not need to be repeated.

Fig. 20 shows the effect of the vibration isolation methods on the sound pressure in room 1, for the case of the wall absorption $\alpha = 0.03$. The floating slab, which only reduces the noise radiation by the room's floor, does not result in significant noise reduction. The box-within-box arrangement is very effective, as it results in an average noise reduction of 10 dB for the total frequency range. The most effective solution is the base isolation of the superstructure, where the noise reduction is about 20 dB in the higher frequency range.

5. Conclusions

A numerical model has been presented that is capable to predict surface traffic induced vibrations and re-radiated sound in buildings, accounting for a moving vibration source, vibration propagation in a layered ground, dynamic soil–structure interaction and sound radiation into acoustic enclosures.

A numerical example has been used to demonstrate the use of the methods. The structural and acoustic response of a three-story portal frame office building has been calculated up to the frequency limit of 150 Hz.

It has been shown that, for the case of a relative stiff soil with a shear wave velocity of $c_S = 250\,\mathrm{m/s}$, the disregarding of dynamic soil–structure interaction effect and a direct excitation of the flexible foundation gives a good approximation of both the structural vibrations levels and the re-radiated sound with reasonable computational effort. The dominant frequencies of the traffic induced acoustic response are basically determined by the first acoustic resonances of the room. The effect of wall absorption on the sound pressure has been investigated, and above the first acoustic resonance, a difference of 5 dB has been found between typical wall absorptions for concrete and carpeted walls. The room dimensions are found to importantly effect the sound pressure level.

The use of the developed methodology has been demonstrated by modelling different noise-isolation methods. The base isolation of the building has been found as the most effective solution for noise isolation.

The entire presented model has not been validated yet by means of comparison with experimental measurement data. This validation is planned for future work.

Regarding the practical application of such a numerical model, it is very important to notice that the adequate description of all the material properties and structural details are not always available for the engineer. In the higher frequency range, where the wavelength is close to the size of the local soil inhomogenities, a homogeneous or a layered half-space soil model can be insufficient to model wave propagation in the ground. On the receiver side, the loss of contact between the structure and the soil, the dynamic behavior of structural joints or the secondary structures inside the building can have a significant effect on the structural vibrations and ground borne noise in the higher frequency range. The appropriate modelling techniques which take the variability of the model's input data into account, are not incorporated in the current deterministic model yet, but they are a major research issue in the future work.

Acknowledgements

The results presented in this paper have been obtained within a cooperation funded by the Flemish Community and the Hungarian Scholarship Board. Their financial support is gratefully acknowledged.

References

[1] A.V. Metrikine, S.N. Verichev, J. Blauwendraad, Stability of a two-mass oscillator moving on a beam supported by a visco-elastic half-space, *International Journal of Solids and Structures* 42 (2005) 1187–1207.

[2] X. Sheng, C.J.C. Jones, M. Petyt, Ground vibration generated by a harmonic load acting on a railway track, *Journal of Sound and Vibration* 225 (1) (1999) 3–28.

[3] L. Auersch, The excitation of ground vibration by rail traffic: theory of vehicle–track–soil interaction and measurements on high-speed lines, *Journal of Sound and Vibration* 284 (1–2) (2005) 103–132.

[4] C. Madshus, A.M. Kaynia, High-speed railway lines on soft ground: dynamic behaviour at critical train speed, *Journal of Sound and Vibration* 231 (3) (2000) 689–701.

[5] X. Sheng, C.J.C. Jones, M. Petyt, Ground vibration generated by a load moving along a railway track, *Journal of Sound and Vibration* 228 (1) (1999) 129–156.

[6] G. Lombaert, Development and Experimental Validation of a Numerical Model for the Free Field Vibrations Induced by Road Traffic, PhD Thesis, Department of Civil Engineering, K.U. Leuven, 2001.

[7] G. Lombaert, G. Degrande, Experimental validation of a numerical prediction model for free field traffic induced vibrations by in situ experiments, *Soil Dynamics and Earthquake Engineering* 21 (6) (2001) 485–497.

[8] G. Lombaert, G. Degrande, The experimental validation of a numerical model for the prediction of the vibrations in the free field produced by road traffic, *Journal of Sound and Vibration* 262 (2003) 309–331.

[9] G. Lombaert, G. Degrande, J. Kogut, S. François, The experimental validation of a numerical model for the prediction of railway induced vibrations, *Journal of Sound and Vibration* 297 (3–5) (2006) 512–535.

[10] D. Aubry, D. Clouteau, A subdomain approach to dynamic soil–structure interaction, in: V. Davidovici, R.W. Clough (Eds.), *Recent Advances in Earthquake Engineering and Structural Dynamics*, Ouest Editions/AFPS, Nantes, 1992, pp. 251–272.

[11] D. Clouteau, *MISS Revision 6.2*, *Manuel Scientifique*. Laboratoire de Mécanique des Sols, Structures et Matériaux, Ecole Centrale de Paris, 1999.

[12] L. Pyl, Development and Experimental Validation of a Numerical Model for Traffic Induced Vibrations in Buildings, PhD Thesis, Department of Civil Engineering, K.U. Leuven, 2004.

[13] L. Pyl, G. Degrande, D. Clouteau, Validation of a source-receiver model for road traffic induced vibrations in buildings. II: receiver model, *Journal of Engineering Mechanics, Proceedings of the ASCE* 130 (12) (2004) 1394–1406.

[14] S. François, L. Pyl, H.R. Masoumi, G. Degrande, The influence of dynamic soil–structure interaction on traffic induced vibrations in buildings, *Soil Dynamics and Earthquake Engineering* (2007), accepted for publication.

[15] P. Fiala, G. Degrande, J. Granát, F. Augusztinovicz, Structural and acoustic response of buildings in the higher frequency range due to surface rail traffic. in: *ICSV13 13th International Congress on Sound and Vibration*, Vienna, Austria, July 2006.

[16] http://www.convurt.com, 2003.

[17] A.B. Nagy, P. Fiala, F. Márki, F. Augusztinovicz, G. Degrande, S. Jacobs, D. Brassenx, Prediction of interior noise in buildings, generated by underground rail traffic, *Journal of Sound and Vibration* 293 (3–5) (2006) 680–690
Proceedings of the 8th International Workshop on Railway Noise, Buxton, UK, 8–11 September 2004.

[18] G. Lombaert, G. Degrande, D. Clouteau, Numerical modelling of free field traffic induced vibrations, *Soil Dynamics and Earthquake Engineering* 19 (7) (2000) 473–488.

[19] J.E. Luco, R.J. Apsel, On the Green's functions for a layered half-space. Part I, *Bulletin of the Seismological Society of America* 4 (1983) 909–929.

[20] G. Degrande, L. Schillemans, Free field vibrations during the passage of a Thalys HST at variable speed, *Journal of Sound and Vibration* 247 (1) (2001) 131–144.

[21] J.P. Wolf, *Dynamic Soil– Structure Interaction*, Prentice-Hall, Englewood Cliffs, NJ, 1985.

[22] R.J. Craig, M. Bampton, Coupling of substructures for dynamic analyses, *AIAA J* 6 (7) (1968) 1313–1319.

[23] S. Rubin, Improved component-mode representation for structural dynamic analysis, *AIAA J* 13 (8) (1975) 995–1006.

[24] T. Gustafsson, H.R. Pota, J. Vance, B.D. Rao, Estimation of acoustical room transfer functions, *Proceedings of the 39th IEEE Conference on Decision and Control*, Sydney, Australia, December 2000.

[25] H.R. Pota, Acoustical room transfer functions without using green's functions, *Proceedings of the 40th IEEE Conference on Decision and Control*, Orlando, FL, December 2001.

[26] H.A. Müller, M. Heckl, *Taschenbuch der Technischen Akustik*, Springer, Berlin, 1994.

[27] C.M. Harris, *Handbook of Acoustical Measurements and Noise Control*, McGraw-Hill, New York, 1991.

[28] T.C. Sabine, *Collected Papers on Acoustics*, Peninsula Publishing, Los Altos, 1993.